Available online at www.sciencedirect.com
SCIENCE DIRECT
Journal of Catalysis 230 (2005) 158–165
JOURNAL OF CATALYSIS
www.elsevier.com/locate/jcat

Visible-light photooxidation of trichloroethylene by Cr–Al-MCM-41

Shalini Rodrigues, Koodali T. Ranjit, S. Uma, Igor N. Martyanov, K.J. Klabunde *

Department of Chemistry, Kansas State University, Manhattan, KS 66506, USA

Received 29 June 2004; revised 11 October 2004; accepted 29 November 2004

Abstract

In the present study, the photooxidation of gaseous trichloroethylene (TCE) was performed on Cr–Al-MCM-41 (predominantly a SiO_2 framework) under visible light and UV light. This mesoporous Cr-containing MCM-41 material is a promising photocatalyst and exhibits excellent photoactivity. Moreover, the products of photooxidation under visible light are similar to those under UV-light illumination. The photocatalysis process occurs on isolated Cr^{6+} ions supported on a predominantly SiO_2 framework. A possible mechanism leading to the photooxidation of TCE together with the detection of intermediates by gas chromatography-mass spectrometry is reported here.

Keywords: Photocatalysis; Visible light; UV irradiation; Mesoporous; Trichloroethylene; Cr–Al-MCM-41

1. Introduction

The increasing contamination of land, water, and air has raised serious environmental problems [1–9]. To reduce the impact of environmental pollution, many efforts have been made in green chemistry and purification technologies. Heterogeneous photocatalytic oxidation is a promising technology for the degradation of volatile organic compounds. The photocatalytic degradation of organic pollutants with the use of TiO_2 has been demonstrated to be successful in various remediation systems of polluted water and air [1,3–6]. It is well known that in the presence of atmospheric oxygen and at room temperature, chlorinated molecules undergo progressive oxidation to complete mineralization, resulting in the formation of CO_2, H_2O, and HCl. Although TiO_2 is very popular as a photocatalyst, it suffers from a lack of visible-light absorption. A chemical process for the degradation of chlorinated organics should yield innocuous products such as CO_2 and HCl that are expected from complete mineralization. There has been active interest in the photooxidation of trichloroethylene (TCE) with the use of TiO_2 [10–15]. It is the most common and abundant pollutant in groundwater in the United States. Previous studies [11–13] have shown that a significant amounts of toxic by-products were formed in the photooxidation of TCE with the use of TiO_2 both in aqueous solution and in the gas phase. The photocatalytic oxidation kinetics of trichloroethylene over titania exhibits complex dependences of the reaction rate on TCE, O_2, and H_2O partial pressure [16]. O_2 is an electron-trapping molecule and was found to be indispensable for photooxidation reactions [1,17–19]. Studies have suggested that the role of O_2 may not be limited to electron trapping [1,4,17–21].

The photocatalytic degradation of TCE vapor has been investigated with various gas mixtures, and several reactor configurations have been used near ambient temperatures and pressure [22–26]. It was experimentally observed that TCE could be oxidized to CO_2 and HCl directly in a photolytic way. However, Li et al. [27] indicated that ultraviolet light was necessary for TCE degradation. In studies of TCE oxidation on TiO_2 in aqueous solution, Pruden and Ollis [28] suggested that hydroxyl radicals initiated the reaction and that dichloroacetaldehyde (DCAAD) is formed as an intermediate. Glaze et al. [13] argued that in addition to the $OH^{\cdot}$ initiated oxidative reaction channels, a parallel reductive pathway involving conduction-band electrons of TiO_2 also plays an important role. In studies of TiO_2 photocatalyzed gaseous TCE oxidation, Anderson et al. [29] pro-

* Corresponding author. Fax: (785) 532 6666.
E-mail address: kenjk@ksu.edu (K.J. Klabunde).

0021-9517/$ – see front matter © 2004 Published by Elsevier Inc.
doi:10.1016/j.jcat.2004.11.044

posed a mechanism involving OH· and a monochloroacetate as an intermediate. Phillips and Raupp [10] suggested that OH· or hydroperoxide radical initiated the reaction that involved DCAAD as an intermediate. In contrast, Nimlos et al. [11,30] suggested that TCE is oxidized in a chain reaction initiated by chlorine atoms. Thus, various mechanisms are currently proposed for TCE photooxidation on TiO_2 surfaces.

Transition-metal-containing mesoporous silicates MCM-41 and aluminosilicates Al-MCM-41 with high surface area are applied in the field of catalysis and have recently been used as photocatalysts. The choice of Al-MCM-41 as the support in the present study was based on the fact that Al-MCM-41 exhibits higher hydrothermal stability compared with pure siliceous MCM-41. We are also interested in the use of these Al-MCM-41 supports as photocatalysts for the remediation of dyes and surfactants (reactions to be carried out in aqueous medium), and hence Al-MCM-41 was chosen as the support. In addition, the incorporation of Al into the framework of MCM-41 generally improves the acidity and ion-exchange capacity of MCM-41, which are crucial properties for catalysts. The use of Cr–Al-MCM-41 as a photocatalyst has already been reported for the decomposition of acetaldehyde under both visible light and UV irradiation [31]. In the present work, the photooxidation of gaseous trichloroethylene on Cr–Al-MCM-41 has been carried out under both visible light and UV radiation. Cr–Al-MCM-41 shows excellent photoactivity under UV-light illumination, but most importantly it also exhibits photoactivity in the visible region, thus making it a more versatile photocatalyst. We observe that under visible-light irradiation, the products are carbon dioxide and phosgene. A possible mechanism leading to the photooxidation of TCE together with the detection of intermediates by GC-MS is reported here. The main objective of this study is to emphasize the importance of our photocatalyst, which is effective for the degradation of volatile chlorinated organics under visible-light irradiation.

2. Experimental

2.1. Synthesis

Commercial cetyltrimethylammonium bromide (CTAB) (Alfa Aesar), tetraethoxy ortho silicate (Aldrich), $Cr(NO_3)_3$ (Alfa Aesar), $Al(NO_3)_3$ (Alfa Aesar), diethylamine (Aldrich), and NH_3 ($\sim$ 25 wt%; Fisher) were used as received for Cr–Al-MCM-41 synthesis. Trichloroethylene (Aldrich) was used as received for photocatalytic measurements. Cr–Al-MCM-41 materials with different chromium content (Si/Cr = 100, 80, 40, 20) were prepared by a co-assembly route with a procedure reported earlier [31]. For Cr–Al-MCM-41 synthesis, the co-assembly process can occur with the involvement of surfactant cations, aluminosilicate species, and an ammonia coordinated transition metal complex, $M(NH_3)_n^{2+}$, where M = Cr and $n = 4, 6$. The gel has a molar composition of 1 SiO_2:x_1 Al_2O_3:2.5x_2 Cr^{3+}:20x_1 NH_4OH:0.14 CTAB:2.4 Et_2NH:100 H_2O ($x_1 = 0.02$ and $0.01 < x_2 < 0.05$). Synthesis of Cr–Al-MCM-41 (Si/Cr = 20) was carried out as follows: 10 ml of diethylamine solution (Et_2NH) was added to a solution containing 72 ml of deionized water, 2.04 g of cetyltrimethylammonium bromide (CTAB), and 0.6 g of $Al(NO_3)_3 \cdot 9H_2O$ and stirred vigorously. Then 0.320 g of $Cr(NO_3)_3$ in 3.6 mL of NH_4OH (25 wt% NH_3) was added to the above mixture. The resulting solution was stirred, and to this 8.9 ml of tetraethylorthosilicate (TEOS) was added dropwise. Finally the mixture was stirred at room temperature for 4 h, followed by static heating at 110 °C for 4 days in a 250-ml polypropylene container. The product obtained was filtered, washed with water, and dried in air at 100 °C overnight. To remove the surfactant, the samples were calcined in air at 630 °C at a heating rate of 1 °C/min. The resulting product was pale yellow in color. Et_2NH is basic enough to form MCM-41 while also enabling the dissolution of the aluminum source, thus readily allowing incorporation of the Al^{3+} ions into the framework. It is this feature in the synthesis that allows the introduction of various transition metal cations into the reaction media. Ammonia is used in the procedure to form complex cations with the transition-metal ions, thus preventing precipitation under basic conditions. With calcination, the surfactant molecule is eventually removed, and the formation of a well-dispersed transition metal oxide phase occurs.

2.2. Characterization

X-ray diffractograms (XRDs) were used to identify the crystal phase of the transition metal incorporated Al-MCM-41. XRDs of the samples were recorded on a Scintag diffractometer with Cu-K_α radiation with a wavelength of 1.5418 Å. Transition-metal-containing Al-MCM-41 powders were analyzed from 2° to 8° (2θ) with a step size of 0.01° to assess the crystallinity of the samples under study. N_2 adsorption–desorption isotherms were obtained at liquid nitrogen temperature (77 K) on a NOVA 1000 Series apparatus. The specific surface areas were calculated according to the Brunauer–Emmett–Teller (BET) method. The pore size distributions were calculated from the desorption curves. The Barett–Joyner–Halenda (BJH) method was used to determine the pore volume (V_{BJH}) and pore size (D_{BJH}). The diffuse reflectance spectra of the samples were recorded in the range of 200–800 nm on a Cary 500 Scan UV–vis NIR spectrophotometer with an integrating sphere attachment. For the electron spin resonance (ESR) experiments, the samples were placed in a standard borosilicate glass ESR tube. The samples were degassed at different temperatures and allowed to cool to room temperature. The tubes were then flame sealed, and the ESR was subsequently recorded. The ESR spectra were recorded with the use of an X band ERS-221 spectrometer at 100-kHz field modulation and low microwave power to avoid power saturation. A homemade computer program (EPR-CAD) was used to

process the experimental data. Photocatalytic experiments were carried out in a cylindrical cell (305 mL/cc total volume). This cell is made of glass and has a quartz window. The Cr–Al-MCM-41 sample (25 mg) was pressed onto Al mesh to create a uniform surface. The experiments were performed at 25 ± 2 °C with stirring. The required amount of trichloroethylene (35 µL) in a gaseous mixture was injected into the injection port for GC-MS analysis. After the TCE concentration was stabilized, the lamp was turned on and the products were analyzed periodically (every 10 min) with GC-MS.

2.3. Quantitative and qualitative analysis

A gas chromatograph equipped with a mass selective detector (GC-MS-QP5000 from Shimadzu) was used for qualitative and quantitative analysis. The following method was used for qualitative identification and quantification of analyzed gaseous reaction products in the present study. Thirty-five microliters of gaseous mixture to be analyzed was injected into the GCMS injection port and kept at 150 °C. The column temperature was maintained at 40 °C. We identified the separated products by comparing experimental and reference mass spectra, following the characteristic masses, and comparing retention times of reaction products with the retention times of pure compounds. Photocatalytic testing of TCE was carried out with a combination of two VIS-NIR long-pass filters (400 nm) and a colored glass filter (> 420 nm) to eliminate ultraviolet radiation during visible-light experiments. Broadband illumination was used in all of the UV experiments. The reaction temperature was maintained at 25 °C. The UV source was a 1000-W high-pressure mercury arc lamp (Oriel Corp.).

3. Results

3.1. XRD and N_2 adsorption studies

A series of Cr–Al-MCM-41 with varying concentrations of Cr^{3+} was prepared by a co-assembly route [31]; these had surface areas greater than 1000 m^2/g. XRD patterns of the calcined Cr–Al-MCM-41 (Si/Cr = 100, 80, 40, and 20) (Fig. 1) are consistent with earlier reports [32–34] indicating a hexagonal structure for these materials. As the concentration of chromium ion in the mesoporous material was increased, there was a slight decrease in the crystallinity. For Cr–Al-MCM-41 (Si/Cr = 20), there was a considerable decrease in the crystallinity, and higher order reflections corresponding to d(210) and d(220) were not observed. Table 1 lists surface areas, pore volumes, and pore sizes for Cr–Al-MCM-41 with various contents of Cr. In general, an increase in the Cr content decreases the surface area; however, for the samples with Si/Cr = 100 and 80, the surface areas were similar. The Si/Cr ratios in the gel and in the final dry powder as determined by SEM-EDXA analysis were comparable

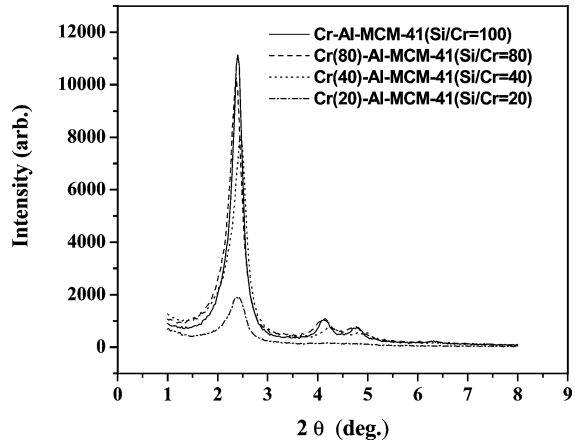

Fig. 1. X-ray powder diffraction pattern of Cr–Al-MCM-41 with Si/Cr = 100, 80, 40, and 20. The observed peaks are due to the MCM-41 structure. The samples were calcined at 630 °C.

Table 1
Surface areas, pore sizes and pore volumes of calcined Cr–Al-MCM-41

Material	Surface area (m^2/g)	Pore size (Å D_{BJH})	Pore volume (cm^3/g)
Cr–Al-MCM-41 (Si/Cr = 100)	1250	30	0.75
Cr–Al-MCM-41 (Si/Cr = 80)	1253	25	0.77
Cr–Al-MCM-41 (Si/Cr = 40)	1180	24	0.72
Cr–Al-MCM-41 (Si/Cr = 20)	1134	24	0.69

(20 gel vs 25 product, 40 gel vs 48 product, 80 gel vs 82 product, and 100 gel vs 96 product).

3.2. UV–vis and ESR of Cr–Al-MCM-41

Fig. 2 shows UV–vis absorption spectra for Cr–Al-MCM-41 (Si/Cr = 100, 80, 40, 20) heated at 100 °C (Fig. 2a) and 630 °C (Fig. 2b). For the samples dried at 100 °C, two broad peaks at 440 and 610 nm characteristic of Cr^{3+} are seen. These peaks can be assigned to the d–d transitions [35,36]. The bands are assigned to $^4A_{2g} \rightarrow {}^4T_{1g}$ and $^4A_{2g} \rightarrow {}^4T_{2g}$ transitions. These transitions can be due to Cr_2O_3 or to isolated Cr^{3+} ions. The absence of any peaks in the XRD due to Cr_2O_3 suggests that the Cr^{3+} ions are well dispersed and isolated in Cr–Al-MCM-41. The Cr^{3+} is oxidized to Cr^{5+} and/or Cr^{6+} when the sample is calcined at 630 °C. The UV–vis spectrum of Cr–Al-MCM-41 calcined at 630 °C shows bands at 275 and 350 nm and a shoulder at 440 nm. The bands at 275 and 350 nm most likely represent the $O^{2-} \rightarrow Cr^{6+}$ charge transfer absorption bands [35,37,38]. However, d–d transition of Cr^{5+} occurs in the same spectral region [39]. The band at 440 nm may be assigned to octahederal Cr^{3+} ions, implying that there is a small amount of unoxidized Cr^{3+} still remaining in the calcined sample. The band at 440 nm may also be attributed to the forbidden charge-transfer band of dichromate species [36]. Thus, with calcination at 630 °C, most of the Cr^{3+} ions are oxidized to Cr^{6+} and or Cr^{5+}.

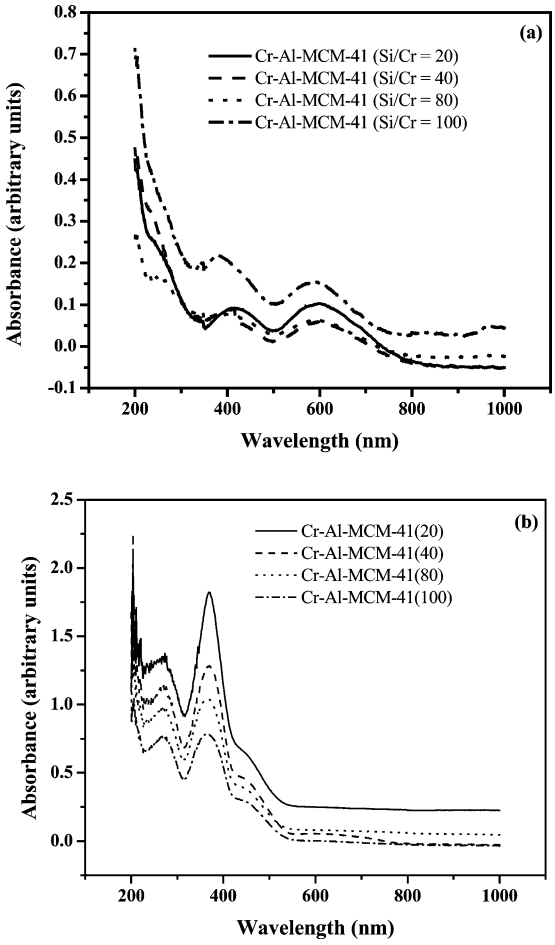

Fig. 2. UV–vis diffuse reflectance spectra of Cr–Al-MCM-41 with various concentrations of Cr^{3+} ions (a) as prepared sample heated at 100 °C and (b) calcined at 630 °C (Si/Cr = 100, 80, 40, and 20).

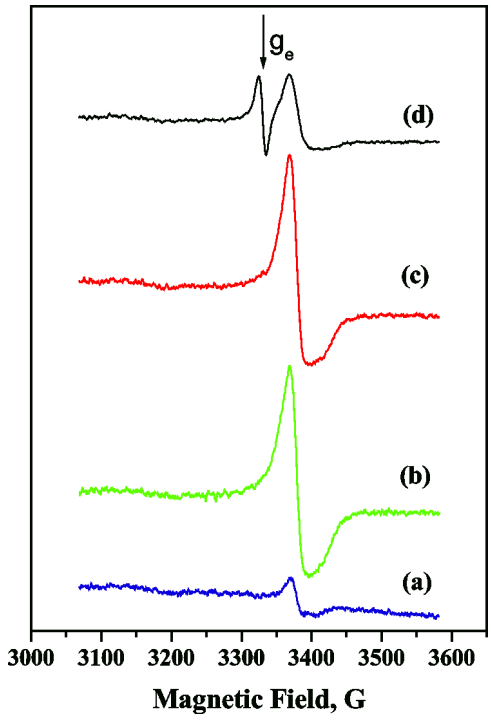

Fig. 3. ESR spectra of Cr–Al-MCM-41 (a) evacuated at room temperature, (b) evacuated at 150 °C, (c) evacuated at 150 °C for 20 h, and (d) evacuated at 350 °C.

The different oxidation states and coordination environments of Cr on oxide supports can be distinguished from each other by a combination of spectroscopic techniques, such as diffuse reflectance spectroscopy (DRS) and ESR [36]. The oxidation state of Cr ions in mesoporous MCM-41 materials has been the subject of investigations by the group of Kevan and Smirniotis [35,40,41]. The ESR spectra of the as-prepared samples before calcination show a broad signal at $g = 1.98$ due to Cr^{3+} that is consistent with earlier reports [40]. Such broad signals with peak-to-peak widths of ~ 500 G have been related to dipolar interactions of Cr^{3+}. Significant broadening of the ESR signals in CrAPSO-5 have been reported by Padylak et al. [42] and Ranjit et al. [43–45]. After Cr–Al-MCM-41 (Si/Cr = 20) is evacuated at room temperature, a weak signal attributed to Cr^{5+} was observed, as shown by Fig. 3a. After evacuation at 150 °C for 1 h, the intensity of the signal due to Cr^{5+} increases substantially, as shown by Fig. 3b. The ESR spectra show a sharp signal at $g_\perp = 1.972$ and a very weak signal at $g_\parallel = 1.952$. The signal at $g_\perp = 1.972$ is assigned to the $g_\perp$ component of Cr^{5+}, possibly in a distorted octahedral or a square-pyramidal coordination. The expected $g_\parallel$ component is normally a weak absorption shape signal. The peak-to-peak width of the signal at $g_\perp = 1.972$, 30 G, is relatively wide, and so the parallel component is poorly resolved. The intensity of this signal is too weak to be detected at room temperature, as has already been observed by several authors [42–45]. The lack of resolution of the $g_\parallel$ component has been attributed in the literature to either a spin exchange effect or a strain broadening process [46]. Additional evacuation for 20 h did not lead to any noticeable change in the ESR spectrum, as shown in Fig. 3c. According to the g equations for square-pyramidal geometry, $g_\perp = g_e - 2\lambda/\Delta_0$ and $g_\parallel = g_e - 8\lambda/\Delta_1$, where λ is the spin–orbit coupling constant of 160 cm^{-1} for Cr^{5+} in an oxide environment [47]. Δ_0 and Δ_1 are the two lowest-energy transitions of calcined, hydrated Cr-MCM-41. The calculated g values are $g_\perp = 1.991$ and $g_\parallel = 1.957$. This $g_\perp$ value is in reasonable agreement with the experimentally observed value of $g_\perp = 1.972$ and $g_\parallel = 1.952$. This supports the assignment of the ESR spectrum to square-pyramidal Cr^{5+}. If distorted octahedral geometry is assumed, $g_\perp < g_\parallel$, which does not agree with the experimentally observed g parameters. When the Cr-MCM-41 sample was evacuated at 350 °C, the g parameters did not change much; however, the intensity of the signal at $g_\perp = 1.972$ decreased approximately 2-fold. A new signal of almost similar intensity appeared near $g = 2.003$ (Fig. 3d). This signal may be due to free electrons of carbonaceous deposits due to the residual template or defects in the framework [48–50]. However, when oxygen was admitted at 7 mm Hg, no changes were observed in the ESR

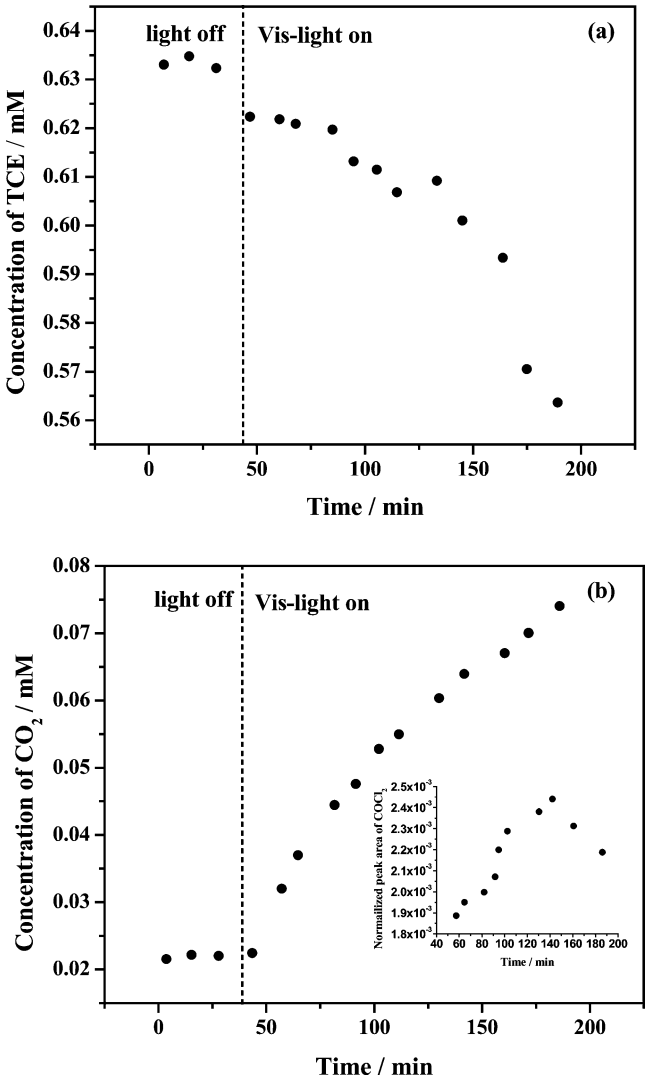

Fig. 4. Graph of concentration vs time for (a) TCE consumption, and (b) CO_2 evolution using Cr–Al-MCM-41 (Si/Cr = 20) under visible-light irradiation. The insert in (b) corresponds to evolution of $COCl_2$.

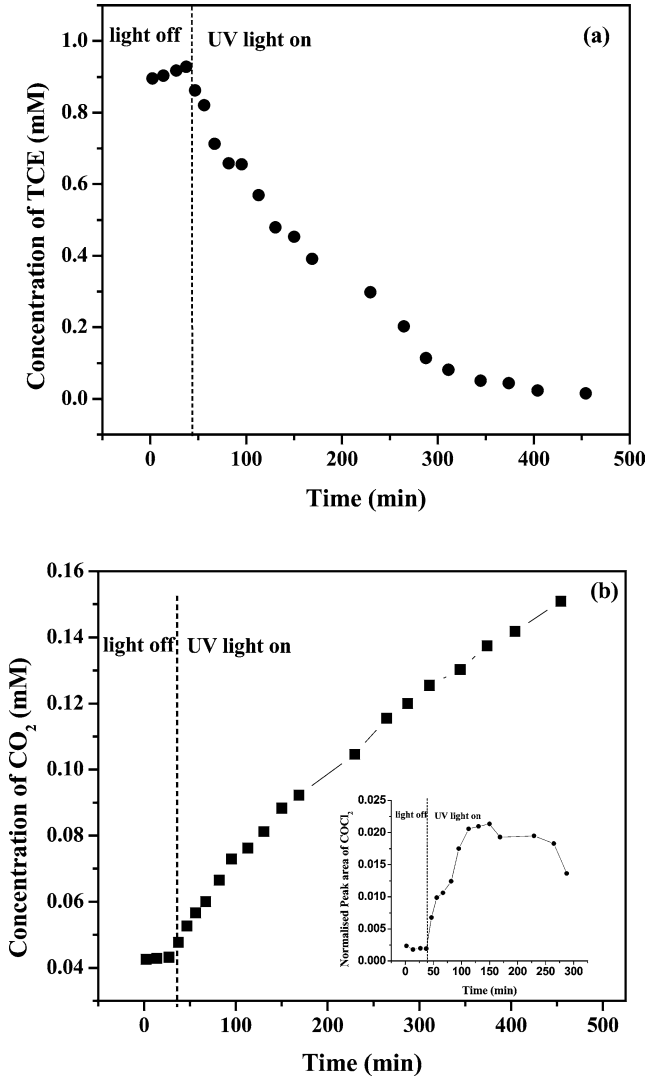

Fig. 5. Graph of concentration vs time for products of TCE photooxidation on Cr–Al-MCM-41 (Si/Cr = 20) under UV irradiation. (a) consumption of TCE, (b) evolution of CO_2. The insert in (b) shows the evolution of $COCl_2$.

spectrum, except for a broadening of the ESR signal. Heating at 200 °C led to the disappearance of the signal and a substantial lowering in the intensity of the Cr^{5+} signal. No signals due to any oxygen radicals were observed at any temperature. This suggests that the signal observed at $g = 2.003$ is a signal of paramagnetic carbonaceous residues. The ESR and DRS results suggest that Cr is present as Cr^{3+} in the as-synthesized sample (heated at 100 °C) and is oxidized mainly to Cr^{6+} and Cr^{5+} in the samples heated at 630 °C.

3.3. Photocatalysis

TCE was illuminated in the absence of the catalyst to ensure the stability of the compound under study. It was observed that there was no change in the concentration of TCE before and after illumination, which shows that the probe molecule is stable under UV irradiation. Upon visible-light illumination and in the presence of the Cr–Al-MCM-41 catalyst (Si/Cr = 20) we found that there was a consumption of TCE together and production of CO_2 and $COCl_2$ as the products of photooxidation (Figs. 4a and 4b). Upon UV-light illumination at 298 K, a rapid consumption of TCE occurred, yielding gaseous primary intermediates: dichloroacetylchloride (DCAC, $CHCl_2COCl$), phosgene, and CO_2. After extensive UV irradiation (> 2 h) it was seen that most of the DCAC had been converted to CO_2 and phosgene. TCE oxidation reaction under UV irradiation is plotted in Figs. 5a and 5b. The concentrations of CO_2, phosgene, and TCE were based on the results from GC-MS. It is clear that DCAC is an intermediate that is later converted into CO_2 and HCl. The intermediate dichloroacetylchloride (DCAC) disappearance proceeds in an apparent first-order fashion after TCE has been consumed. Since a standard for DCAC calibration was not available, its concentration could not be quantitatively determined, although it is qualitatively estimated. Prolonged illumination (> 6 h) under ei-

ther visible or UV light leads to the disappearance of all of the detected reaction intermediates, to yield CO_2 and water as the final reaction products as detected by GC-MS. The HCl formed during the photoreaction probably remains on the surface of the catalyst. The disappearance of TCE and DCAC to below detectable limits, the lack of observation of other organic products, and the observation of only CO_2 demonstrate the complete degradation of TCE by photoassisted heterogeneous catalysis. Similar reaction products have been observed with Degussa P25 TiO_2 by previous workers. The amounts of CO_2 produced after illumination for the initial 30 min in Cr–Al-MCM-41 with $Si/Cr = 100$, 80, 40, and 20 are 20, 24, 32, and 35 mM, respectively. Since the reaction was faster with Cr–Al-MCM-41 with $Si/Cr = 20$, it was chosen for the present study. We are investigating the role of Cr ions and their concentrations in photocatalytic oxidation. The photoassisted heterogeneously catalyzed nature of TCE conversion to DCAC has been reported by Pruden and Ollis [28], suggesting a probable route to the intermediate formation. In homogeneous gas-phase photochemical studies, trichloroethylene and oxygen in UV light yielded dichloroacetyl chloride ($Cl_2HCCOCl$) [51] with no loss of chloride ions. Molecular oxygen is required for complete mineralization of chlorinated hydrocarbons to CO_2 and HCl [52]; the corresponding stoichiometric equation is

$$CCl_2CClH + H_2O + (3/2)O_2 \rightarrow 2CO_2 + 3HCl. \quad (1)$$

However, in the absence of molecular oxygen the reaction was self-poisoning [53]. Diffuse reflectance UV–vis absorption spectra of the spent catalyst obtained after the photocatalytic reaction reveals that all Cr^{6+} is converted to Cr^{3+}. With photoexcitation the holes are utilized for oxidation of TCE and the e^- is trapped by the O_2. Since the reaction is carried out in a closed reactor, once the O_2 concentration is depleted the electron concentration builds up, resulting in the reduction of Cr^{6+} to Cr^{3+}. The photocatalytic reactions were carried out in a closed system, and hence it was not possible to study the affect of O_2 in the Cr^{6+} to Cr^{3+} reduction. However, we are in the process of building a flow reactor to investigate the role of oxygen in the reduction of Cr^{6+} to Cr^{3+}. Preliminary experiments suggest that the presence of oxygen does indeed inhibit the reduction of Cr^{6+} to Cr^{3+}, supporting our hypothesis that the depletion of oxygen results in the Cr^{6+} to Cr^{3+} reduction. However, Cr^{3+} is also a UV photocatalyst, and therefore the photocatalytic reaction does not decrease. TCE photooxidation, when performed under visible light, led to CO_2 production together with $COCl_2$ formation. However, the rate of formation of CO_2 was slow when compared with the reaction under UV light. However, the photooxidation of TCE under visible light and UV light leads to the formation of similar products, and hence they tend to follow a similar reaction mechanism.

4. Possible mechanism for product formation

One may speculate about the possible mechanisms underlying the formation of detected products. Unlike TiO_2, where the photochemistry is well explored for the oxidation of chlorinated volatile organics, the mechanism related to the use of Cr–Al-MCM-41 remains challenging and unexplored.

The DRS results, as discussed earlier, indicate that the chromium ions are highly dispersed and exist in an isolated state on the MCM-41 support. The absence of any peaks corresponding to Cr_2O_3 in Cr–Al-MCM-41 at higher Cr contents (i.e., $Si/Cr = 20$) may suggest two possibilities: (a) the Cr_2O_3 formed may be amorphous or (b) it may be absent. The ratio of $Si/Cr = 20$ is high enough to form Cr_2O_3. Since we do not observe any peaks in the X-ray diffraction patterns, we believe that the Cr^{3+} are well dispersed and isolated. With calcination they form Cr^{6+} and/or Cr^{5+}, as discussed previously. These highly dispersed chromium ions can be excited under UV and/or visible-light radiation to form the corresponding charge-transfer excited state involving an electron transfer from O^{2-} to Cr^{6+} as shown by

$$[Cr^6–O^{2-}] \xrightarrow{h\nu} [Cr^{5+}–O^-]^*. \quad (2)$$

These charge-transfer excited states have high reactivities due to the presence of electron–hole pairs localized next to each other, compared with electron–hole pairs produced in traditional semiconductors such as TiO_2, ZnO, or CdS [54]. Thus, the localized electron–hole pairs under UV and/or visible-light irradiation initiate unique photocatalytic activities that cannot usually be found on dispersed metal oxide semiconductors. Surface hydroxyl groups are ubiquitous on oxide surfaces and especially on MCM-41 types of materials. The density of OH groups on these surfaces has been estimated to be as high as 3 OH/nm^2 at room temperature [55]. Thus, the surface hydroxyl groups can react with the hole produced by excitation to form hydroxyl radicals that are highly reactive:

$$OH^- + h^+ \rightarrow \cdot OH. \quad (3)$$

Preliminary ESR experiments using spin taps indicate the formation of ·OH radicals. However, a thorough ESR study is planned to quantify the amount of hydroxyl radicals produced and their role in the degradation of TCE. The generated ·OH radical then can react with TCE to generate Cl· radicals:

$$Cl_2C{=}CHCl + \cdot OH \rightarrow Cl_2C\cdot–CHClOH, \quad (4)$$

$$Cl_2C\cdot–CHClOH \rightarrow Cl_2C{=}CHOH + Cl\cdot. \quad (5)$$

The Cl· radicals are also highly reactive species and can react with TCE through a chain mechanism as proposed initially by Nimlos [11]:

$$Cl_2C{=}CHCl + Cl\cdot \rightarrow Cl_2HC–CClCl\cdot, \quad (6)$$

$$Cl_2HC–CClCl\cdot + O_2 \rightarrow Cl_2HC–CCl_2OO\cdot, \quad (7)$$

$$2Cl_2HC–CCl_2OO\cdot \rightarrow 2Cl_2HC–CCl_2O\cdot + O_2, \quad (8)$$

$$2Cl_2HC–CCl_2O^{\cdot} \rightarrow Cl_2HC–COCl + Cl^{\cdot}. \quad (9)$$

The DCAC formed as an intermediate decomposes, forming phosgene, carbon dioxide and hydrochloric acid:

$$Cl_2HC–COCl + O_2 \rightarrow COCl_2 + CO_2 + HCl. \quad (10)$$

Prolonged illumination with either visible or UV light leads to the decomposition of $COCl_2$ to CO_2.

5. Conclusions

Photocatalytic oxidation of trichloroethylene over Cr–Al-MCM-41 yields complete mineralization products under UV and visible-light irradiation. The large surface area of this material is populated by the surface hydroxyl groups that participate in the oxidation step. The intermediate species dichloroacetyl chloride undergoes further oxidation to phosgene, carbon dioxide, and HCl. With prolonged illumination phosgene is further oxidized to CO_2 and HCl. Under visible light the Cr^{6+}/Cr^{5+} species happen to be the only photospecies available that are susceptible to visible-wavelength photons, and hence the reaction rate may be slow compared with that in UV light, where, in addition to $Cr^{6+/5+}$, Cr^{3+} ions are also available that are UV active. In conclusion, we have a mesoporous material that is an interesting and promising photocatalyst for volatile chlorinated organics under both visible and UV light.

Acknowledgments

This work was supported by a MURI project (DAAD 19-01-10619) from the U.S. Army Research Office. We thank Dr. Alexander Bedilo for ESR measurements and Dr. Alexander Volodin for useful discussions.

References

[1] M.A. Fox, M.T. Dulay, Chem. Rev. 93 (1993) 341.
[2] D.F. Ollis, H. Al-Ekabi (Eds.), Photocatalytic Purification and Treatment of Water and Air, Elsevier, Amsterdam, 1993.
[3] N. Serpone, E. Pelizzetti (Eds.), Photocatalysis—Fundamentals and Applications, Wiley–Interscience, New York, 1989.
[4] M.R. Hoffmann, S.T. Martin, W. Choi, D.W. Bahnemann, Chem. Rev. 95 (1995) 69.
[5] O. Legrini, E. Oliveros, A.M. Braun, Chem. Rev. 93 (1993) 671.
[6] J. Peral, X. Domenech, D.F. Ollis, J. Chem. Technol. Biotechnol. 70 (1997) 117.
[7] Annual Report on Carcinogenisis Bioassay of Chloroform, National Cancer Institute, Bethseda, MD, March 1, 1976.
[8] M.W. Slein, E.B. Sansome, Degradation of Chemical Carcinogens, Van Nostrand Reinhold, New York, 1979, p. 116.
[9] J.J. Rook, Water Treat. Exam. 23 (1974) 234.
[10] L.A. Phillips, G.B. Raupp, J. Mol. Catal. 77 (1992) 297.
[11] M.R. Nimlos, W.A. Jacoby, D.M. Blake, T.A. Milne, Environ. Sci. Technol. 27 (1993) 732.
[12] W. Holden, A. Marcellino, D. Valic, A.C. Weedon, in: D.F. Ollis, H. Al-Ekabi (Eds.), Photocatalytic Purification and Treatment of Water and Air, Elsevier, Amsterdam, 1993, p. 393.
[13] W.H. Glaze, J.F. Kenneke, J.L. Ferry, Environ. Sci. Technol. 27 (1993) 177.
[14] Y. Zhang, J.C. Crittenden, D.W. Hand, D.L. Perram, Environ. Sci. Technol. 28 (1994) 435.
[15] J.A. Dean, Lange's Handbook of Chemistry, eleventh ed., McGraw-Hill, New York, 1973, p. 4.
[16] A. Dibble, G.B. Raupp, Environ. Sci. Technol. 26 (1992) 492.
[17] G. Lu, A. Linsebigler, J.T. Yates Jr., J. Phys. Chem. 99 (1995) 7626.
[18] C. Wang, A. Heller, H. Gerischer, J. Am. Chem. Soc. 114 (1992) 5230.
[19] J.C.S. Wong, A. Linsebigler, G. Lu, J. Fan, J.T. Yates Jr., J. Phys. Chem. 99 (1995) 335.
[20] A.J. Hoffman, E.R. Carraway, M.R. Hoffmann, Environ. Sci. Technol. 28 (1994) 776.
[21] U. Stafford, K.A. Gray, P.V. Kamat, A. Varma, Chem. Phys. Lett. 55 (1993).
[22] L.A. Dibble, G.B. Raupp, Catal. Lett. 4 (1990) 345.
[23] W.A. Jacoby, M.R. Nimlos, D.M. Blake, R.D. Noble, C.A. Koval, Environ. Sci. Technol. 28 (1994) 1661.
[24] S. Yamazaki-Nishida, K.J. Nagano, L.A. Phillips, S. Cervera-March, M.A. Anderson, J. Photochem. Photobiol. A: Chem. 70 (1993) 95.
[25] E. Berman, J. Dong, in: W.W. Eckenfelder, A.R. Bowers, J.A. Roth (Eds.), The Third International Symposium on Chemical Oxidation: Technology for the Nineties, Vanderbilt University, Nashville, Tennessee, Technomic Publishing, Lancaster, PA, 1993, pp. 183–189.
[26] N.N. Lichtin, M. Avudaithai, Environ. Sci. Technol. 30 (1996) 2014.
[27] G. Li, H. Ma, W. An Chin, J. Catal. 21 (2000) 350.
[28] L.A. Pruden, D.F. Ollis, J. Catal. 82 (1983) 404.
[29] M.A. Anderson, S. Yamazaki-Nishida, S. Cervera-March, in: D.F. Ollis, H. Al-Ekabi (Eds.), Photocatalytic Purification and Treatment of Water and Air, Elsevier, Amsterdam, 1993, p. 405.
[30] M.R. Nimlos, W.A. Jacoby, D.M. Blake, T.A. Milne, in: D.F. Ollis, H. Al-Ekabi (Eds.), Photocatalytic Purification and Treatment of Water and Air, Elsevier, Amsterdam, 1993, p. 387.
[31] S. Rodrigues, S. Uma, I.N. Martyanov, K.J. Klabunde, J. Photochem. Photobiol. A: Chem. 165 (2004) 51.
[32] C.T. Kresge, W.J. Leonowicz, W.J. Roth, J.C. Vartuli, J.S. Beck, Nature 359 (1992) 710.
[33] J.S. Beck, J.C. Vartuli, W.J. Roth, W.J. Leonowicz, C.T. Kresge, K.D. Schmitt, C.T. Chu, D.H. Olson, E.W. Sheppard, S.B. McCulley, J.B. Higgings, J.L. Schlenker, J. Am. Chem. Soc. 114 (1992) 10834.
[34] Z. Luan, J. Xu, H. He, J. Klinowski, L. Kevan, J. Phys. Chem. 100 (1996) 19595.
[35] Z. Zhu, Z. Chang, L. Kevan, J. Phys. Chem. B 103 (1999) 2680.
[36] B.M. Weckhuysen, I.E. Wachs, R.A. Schoonheydt, Chem. Rev. 96 (1996) 3327.
[37] B.M. Weckhuysen, R.R. Rao, J. Pelgrims, R.A. Schoonheydt, P. Bodart, G. Debras, O. Collart, P. Van Der Voort, E.F. Vansant, Chem. Eur. J. 6 (2000) 2960.
[38] P. McCarthy, J. Lauffenburger, P. Skoezny, D. Pohrer, Inorg. Chem. 20 (1981) 1566.
[39] C.D. Garner, J. Kendrick, P. Lambert, F.E. Maabs, I.H. Hiller, Inorg. Chem. 15 (1976) 1287.
[40] S. Sinlapadech, R. Koodali, R.M. Krishna, L. Kevan, J. Phys. Chem. B 106 (2002) 6251.
[41] E.P. Reddy, L. Davydov, P.G. Smirniotis, J. Phys. Chem. B 106 (2002) 3394.
[42] B.V. Padylak, J. Kornatowski, G. Zadrozna, M. Rozwadowski, A. Gutsze, J. Phys. Chem. A 104 (2000) 11837.
[43] K.T. Ranjit, L. Kevan, J. Phys. Chem. B 107 (2003) 2610.
[44] K.T. Ranjit, L. Kevan, Phys. Chem. Chem. Phys. 3 (2001) 2921.
[45] K.T. Ranjit, L. Kevan, J. Phys. Chem. B 106 (2002) 9306.
[46] A.K. Cage, L. Hassan, J. Pardi, L.C. Krzystek, N.S. Brunel, J. Dalal, Magn. Reson. 124 (1997) 495.
[47] D. Kivelson, S.K. Lee, J. Chem. Phys. 41 (1964) 1896.
[48] M. Huang, J. Yao, S. Xu, Ch. Meng, Zeolites 12 (1992) 810.
[49] A.M. Prakash, T. Wasowicz, L. Kevan, J. Phys. Chem. B 101 (1997) 1985.

[50] A.M. Prakash, L. Kevan, J. Phys. Chem. 100 (1996) 19587.
[51] E.M. Huntress, The Preparation, Properties, Chemical Behaviour and Identification of Chlorine Organic Compounds: Tables of Data on Selected Compounds of Order III, Wiley, New York, 1948, p. 611.
[52] C.-Y. Hsiao, C.-Y. Lee, D.F. Ollis, J. Catal. 82 (1982) 418.
[53] K.I. Hadjiivanov, D.G. Klissurski, Chem. Soc. Rev. 25 (1996) 61.
[54] M. Matsuoka, M. Anpo, J. Photochem. Photobiol. C: Photochem. Rev. 3 (2003) 225.
[55] X.S. Zhao, G.Q. Lu, A.J. Whittaker, G.J. Millar, H.Y. Zhu, J. Phys. Chem. B 101 (1997) 6525.